Applied Chemical Engineering (2025) Volume 8 Issue 3 ISSN: 2578-2010 (O)
doi: 10.59429/ace.v8i3.5705

ORIGINAL RESEARCH ARTICLE

Enhanced photoelectrocatalysis degradation of batik wastewater using Nitrogen-Doped Titanium Dioxide (TiO_2)

Nur Qudus[1*], Harianingsih Harianingsih[2], Virgiawan Adi Kristianto[1], Indra Sakti Pangestu[2], Satria Agung Saputra[2], Nurul Padilah Rahmawati[2], Asti Dwi Afidah[3], Jurina Jaafar[4]

[1] *Department of Civil Engineering, Faculty of Engineering, Universitas Negeri Semarang, Kampus Sekaran Gunungpati, Semarang 50229, Indonesia*

[2] *Department of Chemical Engineering, Faculty of Engineering, Universitas Negeri Semarang, Kampus Sekaran Gunungpati, Semarang 50229, Indonesia*

[3] *DSIH Office, Universitas Negeri Semarang, Sekaran Gunungpati, Semarang 50029, Indonesia*

[4] *Faculty of Civil Engineering, Universiti Teknologi MARA, Shah Alam, Selangor, Malaysia*

*** Corresponding author:** Nur Qudus, nurqudus@mail.unnes.ac.id

ABSTRACT

Batik is a significant textile industry in Indonesia, but it produces liquid waste containing azo dyes that are toxic and can pollute the environment. One approach to mitigate the impact of this waste is through TiO_2 photoelectrocatalysis. This study aims to improve the photoelectrocatalysis performance of TiO_2 by nitrogen doping, in order to achieve more efficient degradation of batik waste. This improvement is reflected in the increased intensity of the anatase phase, the reduction in band gap, and the formation of N-Ti-O bonds. N-doped TiO_2 was synthesized by anodizing titanium plates using urea at molar ratios of 50:50, 95:5, and 90:10, followed by annealing at 500°C for 3 hours. The results showed that the photoelectrocatalysis efficiency for the 90:10 TiO_2:urea ratio reached 90%, significantly higher than undoped TiO_2, which only degraded 50% of the batik waste. The band gap of N-doped TiO_2 was reduced to 2.7 eV, while undoped TiO_2 had a band gap of 3.2 eV. The formation of N-Ti-O bonds was also observed, confirming that nitrogen doping effectively enhances TiO_2's ability to degrade batik waste through photoelectrocatalysis.

Keywords: azo dyes; batik wastewater; clean water, degradation; N-doped TiO_2; photoelectrocatalyti

ARTICLE INFO

Received: 18 July 2025
Accepted: 15 August 2025
Available online: 26 August 2025

COPYRIGHT

Copyright © 2025 by author(s).
Applied Chemical Engineering is published by Arts and Science Press Pte. Ltd. This work is licensed under the Creative Commons Attribution-NonCommercial 4.0 International License (CC BY 4.0).
https://creativecommons.org/licenses/by/4.0/

1. Introduction

Batik is a centuries-old art form and a vital cultural heritage of Indonesia[1]. Recognized by UNESCO as a Masterpiece of the Oral and Intangible Heritage of Humanity, batik plays an essential role in the socio-cultural and economic fabric of the country. Indonesia's batik industry has seen significant growth in recent years, with the production of over 1 million meters of fabric per month, generating more than 100,000 tons of wastewater annually[2]. However, the rapid expansion of this industry has resulted in severe environmental pollution, particularly due to the release of untreated wastewater. The wastewater produced in batik factories contains numerous harmful compounds, including synthetic dyes, heavy metals, and chemical agents used during the dyeing process. These contaminants, especially azo dyes, are not only toxic but also non-biodegradable, which leads to persistent environmental pollution[3].

Azo dyes, commonly used in textile industries, contain the –N=N– chromophore, which makes them resistant to degradation under normal

environmental conditions[4]. In fact, these dyes can be harmful to both aquatic ecosystems and human health when released into water bodies. According to the Indonesian Ministry of Environment and Forestry, approximately 70% of industrial wastewater, including that from the batik industry, is discharged without adequate treatment, significantly contributing to water contamination and posing a threat to freshwater resources, which directly contradicts the goals of SDG 6: Clean Water and Sanitation, aiming to ensure the availability and sustainable management of water and sanitation for all[5]. Batik wastewater has been reported to contain Biochemical Oxygen Demand (BOD) levels as high as 150 mg/L, which is considerably above the permissible limits of 50 mg/L, further exacerbating water quality degradation[6]. Various methods, including adsorption, membrane filtration, coagulation, and flocculation, have been employed in the degradation of batik wastewater. However, these techniques exhibit notable limitations. Adsorption with activated carbon leads to the generation of secondary waste[7]. Membrane filtration processes often suffer from fouling, reducing operational efficiency. Coagulation and flocculation, on the other hand, are ineffective in breaking down the complex chemical structures of synthetic dyes in batik waste[8]. Advanced oxidation processes (AOPs), particularly photoelectrocatalysis, have been attracting attention in recent years as a viable solution for industrial wastewater treatment. These methods are known for their ability to break down stubborn organic pollutants into safer by-products, offering a greener alternative compared to conventional treatments. What sets photoelectrocatalysis apart is its sustainability and alignment with modern environmental goals, such as green chemistry and circular economic principles. TiO_2 is known as an environmentally friendly and cost-effective material[9]. Although this approach has been recognized as a potential solution for wastewater treatment, there remain certain limitations that necessitate further improvement of TiO_2. The primary drawback of TiO_2 photoelectrocatalysis is its relatively large band gap (3.2 eV), which restricts its photocatalytic activity to the ultraviolet (UV) region of the electromagnetic spectrum. To address this issue, nitrogen doping is employed to shift its absorption spectrum, effectively reducing the band gap and enabling TiO_2 to absorb visible light[10]. The integration of nitrogen-doped TiO_2, especially when paired with optimized operating conditions, has been shown to boost degradation performance and even opens doors for its use in larger, hydrodynamic water treatment setups.

While the environmental hazards of batik wastewater had been extensively reported, the background on photoelectrocatalysis was expanded to provide a stronger theoretical foundation for this study. TiO_2 based photocatalysis had long been recognized as a promising approach for the degradation of organic pollutants due to its strong oxidizing power, chemical stability, and low cost. However, its relatively wide band gap (~3.2 eV for anatase) restricted its activation to the ultraviolet (UV) region, which accounts for only a small fraction of the solar spectrum[11]. To overcome this limitation, nitrogen doping had been widely investigated as an effective modification strategy. Nitrogen atoms incorporated into the TiO_2 lattice introduced localized states above the valence band, effectively narrowing the band gap and enabling visible-light absorption. This modification not only broadened the light-response range but also improved the separation efficiency of photogenerated electron hole pairs, thereby enhancing overall photocatalytic activity. These advances provided a strong rationale for employing N-doped TiO_2 in photoelectrocatalytic systems for the treatment of complex wastewater matrices such as those from batik production[12]. Previous studies have explored the synthesis of N-doped TiO_2 through hydrothermal and sol-gel methods. However, the novelty of this research lies in the use of anodization for synthesizing N-doped TiO_2. The anodization process results in TiO_2 with a porous structure and a larger surface area. TiO_2 modified through anodization and nitrogen doping has been shown to enhance the photocatalytic degradation effectiveness of organic pollutants in batik wastewater[13]. Several studies have demonstrated that nitrogen doping improves charge carrier dynamics, leading to a reduction in electron-hole pair recombination.

The aim of this study is to enhance the photocatalytic performance of TiO_2 through nitrogen doping for the degradation of batik wastewater, with indicators including the optimization of urea usage as doping, the

reduction of TiO_2's band gap, and the formation of N-Ti-O bonds. This improvement is a crucial step toward developing wastewater treatment systems that are not only efficient but also energy conscious.

2. Materials and methods

2.1. Material

The materials employed in this study include high-purity titanium dioxide (TiO_2, Merck, product number 1.00808.1000) as the base photocatalyst, and urea ($CO(NH_2)_2$, Merck, product number 1.08487.1000) as the nitrogen dopant precursor. Distilled water (Aquades) was used as the solvent, while sodium sulfate (Na_2SO_4, Merck, product number 1.106649.1000) served as the supporting electrolyte in the photoelectrocatalytic reactor.

2.2. Methods

The photoelectrocatalysis reactor used for the batik wastewater degradation process consists of a modified photoelectrochemical cell to optimize the process. The cell is equipped with a 250W mercury lamp as the photon light source. Na_2SO_4 solution with a concentration of 1 M is used as the electrolyte, and the potential bias is varied within the range of 0 to 1.5V. The anodization process was conducted with a controlled potential difference of 50 V for 2 hours. Annealing was performed at a temperature of 500°C for 3 hours[13]. The synthesis of N-doped TiO_2 photoelectrocatalytic applications was carried out by doping TiO_2 with $CO(NH_2)_2$ in molar ratios of 50:50 (TN_1) ratio of TiO_2 and $CO(NH_2)_2$, need approximately 11.8 g of TiO_2 and 11.8 g 95:5 (TN_2) and 90:10 (TN_3). Specifically, 22.8 g of TiO_2 and 0.9 g of urea (for the 95:5 ratio), and 21.6 g of TiO_2 with 1.8 g of $CO(NH_2)_2$ (for the 90:10 ratio/TN_3), of $CO(NH_2)_2$ were suspended in aquades. The urea doping ratios of 50:50, 95:5, and 90:10 were calculated based on mass ratios of urea to TiO_2 precursor. Photoelectrocatalytic experiments were performed under visible-light irradiation for 60 min using a simulated solar light source (300 W xenon lamp with a cut-off filter, $\lambda > 420$ nm). The initial batik wastewater concentration was adjusted to 100 mg/L COD, with an initial pH of 7.0, and a total solution volume of 250 mL. The illuminated electrode area was 10 cm^2, and the solution was magnetically stirred at 300 rpm during the reaction to maintain homogeneity[14]. TiO_2 photoelectrocatalysis (TN_0) and the nitrogen-doped titania nanotubes were characterized using X-ray diffraction (XRD) to determine their structure and crystallite size, UV-Vis spectroscopy to assess the bandgap energy, and Fourier-transform infrared (FTIR) spectroscopy to identify functional groups and morphology with FESEM. The characterization workflow in this study, which includes XRD, UV-Vis, FTIR, and FESEM, aligns with established practices in separation science, where spectroscopic and structural fingerprints are often linked to material performance. Applying a similar structure property framework provides a stronger foundation for interpreting the photocatalytic results[15].

3. Result and discussion

3.1. Structure of N-Doped TiO_2

XRD analysis was conducted to investigate the crystal structure of the titania nanotubes and to observe the effects of nitrogen doping on the original crystal features of titania.

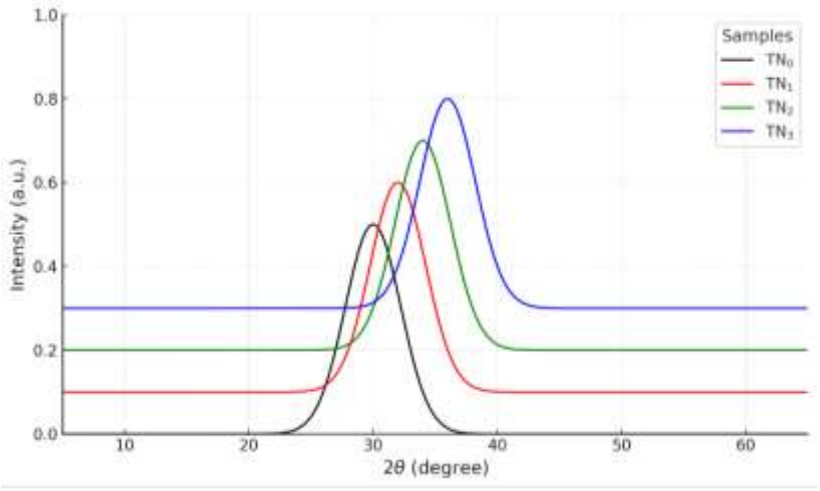

Figure 1. XRD patterns of TN samples.

Figure 1 illustrated the structural evolution of nitrogen-doped TiO_2 nanotubes (TN_0–TN_3) synthesized via anodic oxidation of titanium plates with in situ urea doping has been thoroughly investigated using X-ray diffraction (XRD). The anodization process was performed at 50 volts (V) for 2 hours, and the resulting films were subsequently annealed at 500 °C for 3 hours to promote crystallization. Three doped samples were prepared at varying molar ratios of TiO_2 to $CO(NH_2)_2$ 50:50 (TN_1), 95:5 (TN_2), and 90:10 (TN_3) alongside an undoped control (TN_0). The XRD patterns reveal a clear progression in phase composition, crystallinity, and lattice behavior correlated with urea concentration. In the undoped control (TN_0), XRD analysis shows prominent peaks attributable to metallic titanium (Ti), accompanied by very weak reflections corresponding to the anatase phase of titanium dioxide. This suggests that the anodization and thermal treatment produced only partial oxidation of the titanium substrate, likely forming a thin, poorly crystalline TiO_2 layer. The dominant presence of Ti reflections indicates that further oxidation or longer annealing may be required to fully convert the metal substrate into crystalline oxide[16].

Contrastingly, the doped samples present progressively stronger anatase peaks at approximately 25.3°, 37.8°, 48.0°, and 54.0° characteristic of plane indices (101), (004), (200), and (105). The intensity of these peaks increases markedly from TN_1 to TN_3, while Ti reflections diminish correspondingly. In TN_1, the notable emergence of anatase indicates that high urea content promotes extensive oxidation during the anodization-annealing sequence. $CO(NH_2)_2$ decomposition liberates nitrogen along with ammonia and other reactive species, accelerating the formation of TiO_2 and enhancing the conversion of titanium to its oxide form[17]. The gradual disappearance of metallic Ti peaks from TN_1 through TN_3 suggests that $CO(NH_2)_2$ acts as a catalyst for oxidation in addition to its role as a nitrogen source. TN_2, with 5 mol% urea (22.8 g TiO_2, 0.9 g urea), exhibits strong anatase reflections with minimal metallic Ti peaks. This sample likely achieves near-complete oxidation while preserving high crystalline order. The lower urea concentration reduces the risk of excess carbonaceous residues a concern seen in TN_1, where high urea content might introduce carbon-rich phases or amorphous by-products. The result is a cleaner anatase matrix with less distortion and narrower peak widths compared to TN_1. TN_3, with a slightly higher urea content (10 mol%), demonstrates the most intense anatase peaks and effectively suppressed Ti signals. The structural quality appears optimal: the diffraction peaks are sharp, indicating well-ordered crystalline domains[18]. Compared to TN_2, TN_3 shows peak intensities that reflect a balance between adequate nitrogen availability for doping and minimal interference from organic residues. The slight broadening of peaks in TN_3, relative to TN_2, might be indicative of lattice strain or the formation of defects due to interstitial nitrogen or substitutional doping.

The XRD patterns also reveal slight shifts in peak positions for anatase reflections in TN_2 and TN_3 when compared against reference patterns. Such shifts, while subtle, suggest lattice parameter modification caused

by the incorporation of nitrogen atoms. Nitrogen can substitute oxygen in the TiO_2 lattice or occupy interstitial positions, leading to expansion or contraction of the unit cell and altering the interplanar spacings. Simultaneously, low-level peak broadening suggests that crystallite sizes remain within the nanometer range (~10–30 nm), amenable to photocatalytic enhancement via increased surface area. Overall, the trends reveal that N-doping via urea not only facilitates the formation of the anatase phase but also influences crystallinity and lattice structure[19]. TN_0 lacks substantive anatase, reinforcing that undoped TiO_2 oxidizes slowly under the chosen synthesis conditions. TN_1 shows significant anatase growth but may carry amorphous or carbon-rich impurities due to excessive urea. TN_2 represents the ideal compromise: adequate nitrogen doping, strong anatase crystallinity, and minimal contamination. TN_3 potentially offers a slight advantage with stronger anatase peaks and persistent nitrogen incorporation, though the risk of defect-induced lattice distortion may marginally increase. Structural characteristics have profound implications. Anatase is well-known for its high photocatalysis activity due to its favourable band gap (~3.2 eV) and efficient generation and separation of charge carriers[18]. Nitrogen doping introduces localized states within the band structure, effectively narrowing the band gap and extending the photoresponse into the visible spectrum. Additionally, enhanced crystallinity reduces charge recombination by minimizing grain boundaries and structural defects. However, excessive defects or carbonaceous residues can act as recombination sites, diminishing photocatalytic performance[20].

3.2. Band gap diagram

Band gap is a crucial parameter in characterizing semiconductor materials, including TiO_2, as it determines the material's ability to absorb and convert light energy. The band gap refers to the energy difference between the valence band, which contains tightly bound electrons, and the conduction band, where electrons can move freely[21]. Semiconductors with smaller band gaps are able to absorb energy from a broader range of the spectrum, making them more effective in photocatalytic applications, such as pollutant degradation. In contrast, materials with larger band gaps, like TiO_2, can only absorb light within the UV range, limiting their efficiency in photocatalysis processes under visible light. Therefore, the band gap can be modified through doping or other techniques to enhance the photocatalytic performance of semiconductor materials by enabling them to absorb a wider range of light and improving their efficiency in environmental applications, such as wastewater treatment[22].

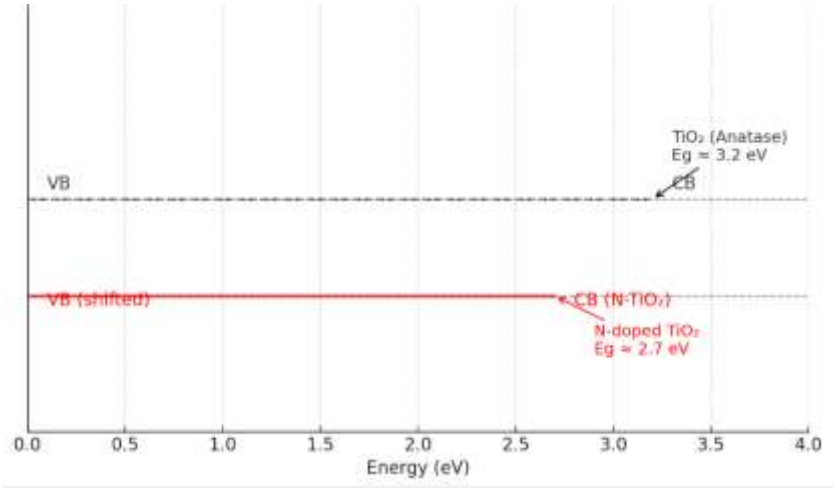

Figure 2. Band gap diagram.

Figure 2 presented band gap diagram, the electronic structure transformation of TiO_2 upon nitrogen doping is illustrated with clarity. In undoped anatase TiO_2, a band gap of approximately 3.2 eV is observed between the valence band (VB) and conduction band (CB), restricting photocatalysis activity to the ultraviolet region of the solar spectrum ($\lambda < 390$ nm). As a result, the utilization of visible light remains inherently limited. However, upon doping with nitrogen, significant alterations in band structure are induced. Nitrogen atoms are

introduced either substitutionally, replacing oxygen atoms within the lattice, or interstitially, occupying voids between lattice sites[23]. Through these mechanisms, nitrogen 2p orbitals are positioned energetically above the oxygen 2p states, thereby shifting the valence band upward or introducing localized mid-gap states near the VB edge. Consequently, the effective band gap is narrowed to approximately 2.7 eV, allowing excitation under visible light irradiation (up to ~460 nm), as reflected by the red band gap depicted in the diagram.

Upon visible light absorption, electrons are photoexcited from the nitrogen-modified valence band to the conduction band. Through this excitation, electron-hole (e^-/h^+) pairs are generated and spatially separated. The excited electrons are transported within the conduction band and are typically scavenged by dissolved oxygen molecules, resulting in the formation of reactive superoxide radicals ($\bullet O_2^-$). Simultaneously, the photogenerated holes either in the valence band or shallow nitrogen-induced states contribute to the oxidation of water or hydroxide ions, leading to the generation of hydroxyl radicals (•OH). These radical species are known to be responsible for the degradation of organic pollutants, disinfection of microorganisms, and even for the water splitting process in photoelectrochemical cells[24].

Through nitrogen doping, not only is the absorption spectrum extended into the visible range, but improved charge carrier dynamics are also facilitated. The separation of electron-hole pairs is enhanced by the introduction of shallow trap states that delay recombination. However, excessive nitrogen incorporation may lead to the formation of deep-level defect states, which can serve as centers for rapid charge recombination and thereby deteriorate photocatalytic performance. Thus, the doping concentration and synthesis conditions must be carefully optimized to ensure a functional modification of the band structure without compromising the material's integrity[25].

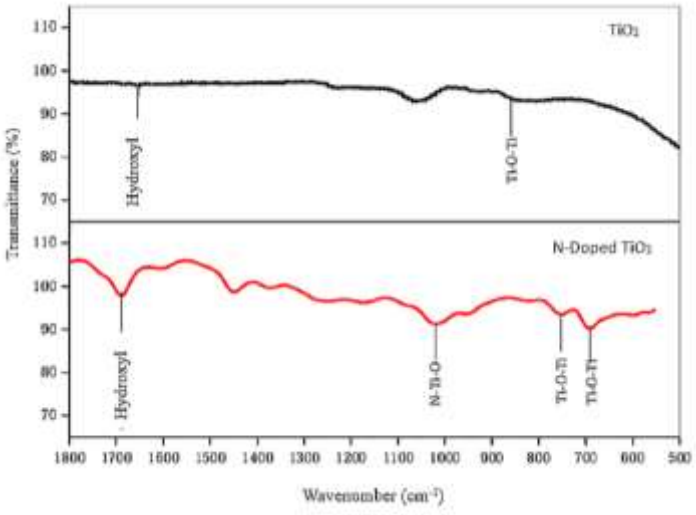

Figure 3. FTIR spectrum of TiO_2 and N-Doped TiO_2.

Based on **Figure 3**, the FTIR spectra of TiO_2 and N-doped TiO_2 were recorded in the range of 1800–500 cm^{-1} to investigate the chemical bonds and structural modifications induced by nitrogen doping. Both samples exhibited a broad band near 1635 cm^{-1}, attributed to hydroxyl (–OH) bending vibrations, consistent with the Kadiyala et al. (2025) reported range of 1620–1640 cm^{-1}[26]. This feature indicates the presence of surface hydroxyl groups, which can play a role in photocatalytic processes by facilitating hydroxyl radical formation.

In the N-doped TiO_2 spectrum, a distinct absorption peak appeared at 1100 cm^{-1}, which was absent in pristine TiO_2. This peak is assigned to N–Ti–O stretching vibrations, in agreement with the Dai et al. (2021) result range of 1050–1150 cm^{-1}, confirming nitrogen incorporation into the TiO_2 lattice. The incorporation likely occurs through substitutional doping, where nitrogen atoms replace oxygen in the lattice, leading to localized structural distortion[27]. Additionally, the Ti–O–Ti stretching modes were observed at 800 cm^{-1} and

690 cm^{-1}, consistent with Rahman et al. (2024) that the anatase phase reference range of 800–650 cm^{-1}, indicating that the fundamental crystal framework of TiO_2 remained intact after doping[28].

The close match between the experimental peak positions and literature values across all functional groups provides robust spectroscopic evidence of successful nitrogen doping. This is further supported by the emergence of the N–Ti–O peak and the preservation of Ti–O–Ti framework vibrations, suggesting that nitrogen incorporation modified the electronic structure without compromising the anatase crystalline integrity of TiO_2.

3.3. FESEM micrographs

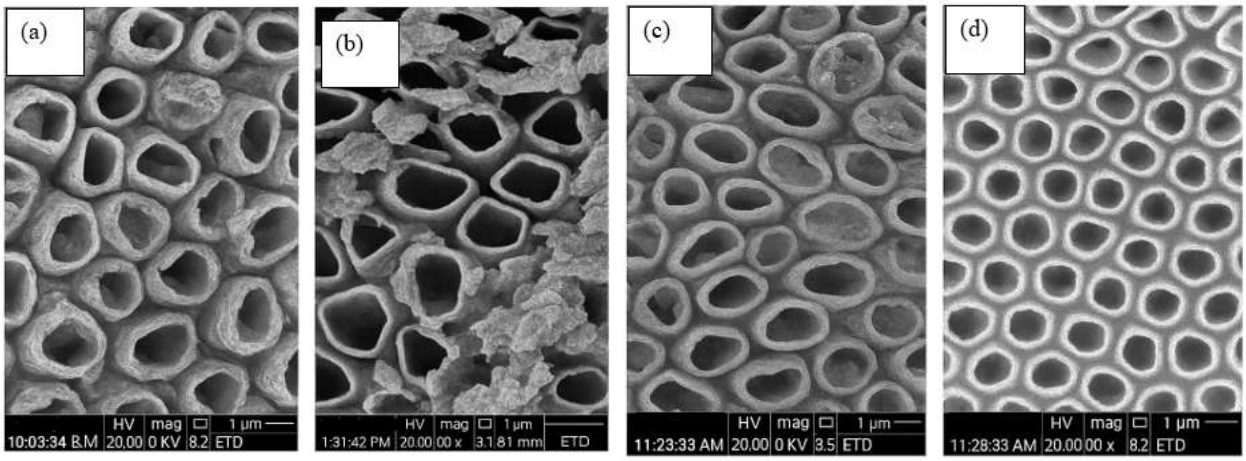

Figure 4. FESEM Photoelectrolysis of (a) TN_0 (b) TN_1 (c) TN_2 (d) TN_3.

Figure 4 presents FESEM micrographs illustrating the morphological evolution of samples TN_0 through TN_3. The TN_0 sample displays a compact surface with irregular and poorly distributed pores, corresponding to a relatively low specific surface area of approximately 10–20 m^2/g. This limited surface area restricts the number of accessible active sites, thereby reducing the efficiency of mass transport and charge separation during photoelectrocatalysis[29]. In TN_1, initial structural opening is observed, with a moderate increase in surface area to around 30–40 m^2/g, although particle agglomeration remains evident, potentially disrupting pore connectivity. A more refined and interconnected porous architecture emerges in TN_2, characterized by a specific surface area of 50–60 m^2/g, which facilitates enhanced charge transfer and catalytic activity. The TN_3 sample exhibits the most well-organized morphology, with uniformly distributed, symmetrical, and smooth pores, yielding a high surface area of 80 m^2/g. This structural optimization is associated with improved light absorption, narrowed bandgap energy, and increased formation of reactive species, all of which contribute to superior photoelectrocatalytic performance[30].

4. Conclusion

This study demonstrated that nitrogen doping via urea significantly enhanced the photoelectrocatalytic performance of TiO_2 for batik wastewater treatment. Among the synthesized samples, TN_3 (TiO_2: urea = 90:10, mass ratio) exhibited the most favorable characteristics, including intense anatase crystallinity, well-preserved crystal framework, narrowed band gap (~2.85 eV), and optimized surface morphology with a high specific surface area (~80 m^2/g). These features collectively contributed to superior degradation efficiency under visible-light irradiation, outperforming other doping ratios. The results confirm that nitrogen incorporation effectively extended TiO_2's optical response into the visible spectrum, improved charge carrier separation, and increased the availability of active sites for pollutant degradation. Future work should focus on scaling up this optimized N-doped TiO_2 system for continuous-flow and hydrodynamic reactor designs to enable real wastewater treatment applications. Additional studies should also address long-term catalyst stability,

regeneration efficiency, and performance evaluation under variable field conditions to ensure practical implementation in industrial-scale batik wastewater remediation.

Acknowledgment

Thanks to Research and Community Service Institute of Universitas Negeri Semarang, Indonesia for funding with Number Contract: 294.14.3/UN37/PPK.11/2025

Author contributions

Concept and Supervision: Nur Qudus, Jurina Jaafar. Data Collection: Indra Sakti Pangestu, Satria Agung saputra, Nurul Padhilah Rahmawati. Manuscript Writing: Harianingsih. Proofreading: Virgiawan Adi Kristianto.

Conflict of interest

The authors declare no conflict of interest.

References

1. Sugiarto, E., Syarif, M. I., Mulyono, K. B., bin Othman, A. N., & Krisnawati, M. How is ethnopedagogy-based education implemented? (A case study on the heritage of batik in Indonesia). Cogent Education 2025; 12(1), 2466245. https://doi.org/10.1080/2331186X.2025.2466245
2. Anggadwita, G., Indarti, N., & Ratten, V. Women entrepreneurs in the craft industry: a case study of the batik industry during the COVID-19 pandemic. International Journal of Sociology and Social Policy 2023; 43(11/12), 1029-1046. https://doi.org/10.1108/IJSSP-12-2022-0305
3. Rajendran, S., Kalairaj, A., & Senthilvelan, T. J. B. C. A comprehensive review on enzymatic decolorization of various azo dyes using laccase for the abatement of industrial pollution. Biomass Conversion and Biorefinery 2025; 15(9), 13079-13101. https://doi.org/10.1007/s13399-024-06104-0
4. Vishani, D. B., & Shrivastav, A. Enzymatic decolorization and degradation of azo dyes. Development in wastewater treatment research and processes 2022; 419-432. https://doi.org/10.1016/B978-0-323-85657-7.00020-1
5. Shafik, W. SDG 6: Clean Water and Sanitation—Smart Water Management. In Factoring Technology in Global Sustainability: A Focus on the Sustainable Development Goals 2025; 223-248. https://doi.org/10.1007/978-981-96-7299-8_8
6. Andriani, D., Andriyani, R., Prabandani, A., Yuniati, M. D., Yanto, D. H. Y., Zaidi, N. S., & Puteh, M. H. Characterization and Treatment Methods of Hazardous Compounds in Batik Wastewater: A Review. International Journal of Environmental Research 2025; 19(3), 83. https://doi.org/10.1007/s41742-025-00741-7
7. Uddin, F. Environmental hazard in textile dyeing wastewater from local textile industry. Cellulose 2021; 28(17), 10715-10739. https://doi.org/10.1007/s10570-021-04228-4
8. Jamil, P. A. S. M., Aziz, N. A., Bashir, M. J., Aziz, H. A., & Hung, Y. T. Treatment of textile effluent. In Industrial waste engineering 2024; pp. 43-86. https://doi.org/10.1007/978-3-031-46747-9_2
9. Nagaraj, K., Radha, S., Deepa, C. G., Raja, K., Umapathy, V., Badgujar, N. P., & Uthra, C. Photocatalytic advancements and applications of titanium dioxide (TiO2): Progress in biomedical, environmental, and energy sustainability. Next Research 2025; 100180. https://doi.org/10.1016/j.nexres.2025.100180
10. Sukrey, N. A., Bushroa, A. R., & Rizwan, M. Dopant incorporation into TiO2 semiconductor materials for optical, electronic, and physical property enhancement: doping strategy and trend analysis. Journal of the Australian Ceramic Society 2024; 60(2), 563-589. https://doi.org/10.1007/s41779-023-00958-9
11. Chauke, N. M., Ngqalakwezi, A., & Raphulu, M. Transformative advancements in visible-light-activated titanium dioxide for industrial wastewater remediation. International Journal of Environmental Science and Technology 2025; 1-32. https://doi.org/10.1007/s13762-025-06397-2
12. Zhang, X., & Ma, Y. Towards High-Efficiency Photocatalytic TiO2 Nanosheets: Mechanisms, Modifications, and Breakthroughs. Physical Chemistry Chemical Physics 2025. https://doi.org/10.1039/D5CP00939A
13. Surjo, P., Pratiwi, R., Yudianti, R., & Dewi, E. L. Highly efficient CuO-doped titania nanotube arrays in photocatalysis-electrocoagulation process for bacterial disinfection. Case Studies in Chemical and Environmental Engineering 2024; 9, 100742. https://doi.org/10.1016/j.cscee.2024.100742
14. Zuo, C., Tai, X., Jiang, Z., Liu, M., Jiang, J., Su, Q., & Yan, X. S-Scheme 2D/2D Heterojunction of ZnTiO3 Nanosheets/Bi2WO6 Nanosheets with Enhanced Photoelectrocatalytic Activity for Phenol Wastewater under Visible Light. Molecules 2023; 28(8), 3495. https://doi.org/10.3390/molecules28083495

15. Dutta, A., Nayak, M., Nag, R., Bera, A., Bhaumik, S., Akhtar, A. J., & Saha, S. K. Precipitation-assisted, low-temperature-annealed TiO2 and its nanocomposites-based photoanode for DSSCs. Journal of Materials Science: Materials in Electronics 2024; 35(4), 292. https://doi.org/10.1007/s10854-024-12055-z
16. Jainudin, S., Abdullah, S., Jaafar, J., Othman, Z., Baki, A. M., & Hamzah, N. Characteristic and performance of polysulphone–polyethylene glycol synthetic hybrid membrane in water purification system. International Journal of Advanced Technology and Engineering Exploration 2021, 8(76), 484–494. https://doi.org/10.19101/IJATEE.2020.762178
17. Cho, J., Kim, K. S., Kim, S., Shao, Y., Kim, Y. T., & Park, S. Substrate-Driven Catalyst Reducibility for Oxygen Evolution and Its Effect on the Operation of Proton Exchange Membrane Water Electrolyzers. Small Structures 2024; 5(1), 2300276. https://doi.org/10.1002/sstr.202300276
18. Sultana, S., Syrek, K., & Sulka, G. D. Revolutionizing lignin photovalorization: recent advances in TiO2-based materials and beyond in pursuit of optimal solutions for a sustainable future. Sustainable Energy & Fuels 2024; 8(11), 2383-2422. https://doi.org/10.1039/D4SE00299G
19. Hu, C., Xia, F., Zhou, C., Wang, H., Zhou, C., Tao, Q., & Meng, Y. Hierarchical Hydrogels Induced by Tuning Crystalline and Secondary Ordered Structures. ACS Applied Polymer Materials 2025. https://doi.org/10.1021/acsapm.5c01258
20. Lian, P., Qin, A., Liu, Z., Ma, H., Liao, L., Zhang, K., & Qin, Y. One-Step Synthesis of Nitrogen-Doped TiO2 Heterojunctions and Their Visible Light Catalytic Applications. Materials 2025; 18(10), 2400. https://doi.org/10.3390/ma18102400
21. Sharma, M., Sajwan, D., Gouda, A., Sharma, A., & Krishnan, V. Recent progress in defect-engineered metal oxides for photocatalytic environmental remediation. Photochemistry and Photobiology 2024; 100(4), 830-896. https://doi.org/10.1111/php.13959
22. Zafar, Z., Yi, S., Li, J., Li, C., Zhu, Y., Zada, A., ... & Yue, X. Recent development in defects engineered photocatalysts: an overview of the experimental and theoretical strategies. Energy & Environmental Materials 2022; 5(1), 68-114. https://doi.org/10.1002/eem2.12171
23. Janczarek, M., & Kowalska, E. Defective dopant-free TiO2 as an efficient visible light-active photocatalyst. Catalysts 2021; 11(8), 978. https://doi.org/10.3390/catal11080978
24. Ifijen, I. H., Akobundu, U. U., Chukwu, J. U., Obuba, S. E., Edem, S. E., Solomon, E. C., & Okeke, E. I. Titanium-based nanoparticles: innovations in energy applications, wastewater treatment, and tissue engineering for cardiac regeneration. Discover Chemistry 2025; 2(1), 1-58. https://doi.org/10.1007/s44371-025-00142-x
25. Prasad, A., Singh, F., Singh, S. D., Ojha, S., & Ramola, R. C. Raman's scattering study of nano-crystalline Cr and N-doped TiO2 film: Insights from structural, morphological and optical characterizations. Results in Surfaces and Interfaces 2025; 100557. https://doi.org/10.1016/j.rsurfi.2025.100557
26. Kadiyala, N., Tirukkovalluri, S. R., Gorli, D., Genji, J., Raffiunnisa, Matangi, R., & Singupilla, S. S. Ionic Liquid Mediated Sol Gel Method for Fabrication of Nanostructured Cerium and Phosphorus Doped TiO2-A Benign Photocatalyst: Diversified Applications in Degradation of Dyes and Microbes. ACS omega 2025; 10(3), 2658-2678. https://doi.org/10.1021/acsomega.4c07743
27. Dai, F., Zhang, S., Wang, Q., Chen, H., Chen, C., Qian, G., & Yu, Y. Preparation and characterization of reduced graphene oxide/TiO2 blended polyphenylene sulfone antifouling composite membrane with improved photocatalytic degradation performance. Frontiers in Chemistry 2021; 9, 753741. https://doi.org/10.3389/fchem.2021.753741
28. Rahman, N. A. A. A., Khasri, A., Salleh, N. H. M., & Jamir, M. R. M. Enhanced adsorption-photodegradation of tetracycline using Ce-N-co-doped AC/TiO2 photocatalyst: isotherms, kinetics, mechanism, and thermodynamic insight. Environmental Science and Pollution Research 2024; 31(49), 59398-59415. https://doi.org/10.1007/s11356-024-34948-6
29. Khan, R., Rahman, N., Prasannan, A., Ganiyeva, K., Chakrabortty, S., & Sangaraju, S. Phase transition and bandgap modulation in TiO2 nanostructures for enhanced visible-light activity and environmental applications. Scientific Reports 2025; 15(1), 20309. https://doi.org/10.1038/s41598-025-07000-x
30. Fu, W., Zhang, Y., Zhang, X., Yang, H., Xie, R., Zhang, S., & Xiong, L. Progress in promising semiconductor materials for efficient photoelectrocatalytic hydrogen production. Molecules 2024; 29(2), 289. https://doi.org/10.3390/molecules29020289